ChemComm
Chemical Communications

Accepted Manuscript

This article can be cited before page numbers have been issued, to do this please use: H. Pang, X. Li, P. Y. Zhu and C. Liu, *Chem. Commun.*, 2019, DOI: 10.1039/C9CC03787J.

ROYAL SOCIETY OF CHEMISTRY

rsc.li/chemcomm

View Article Online
DOI: 10.1039/C9CC03787J

COMMUNICATION

One step synthesis of boron-doped carbon nitride derived from 4-pyridylboronic acid as biosensing platforms for assessment of food safety

Received 00th January 20xx,
Accepted 00th January 20xx

DOI: 10.1039/x0xx00000x

Xiaxia Li,[a] Peiyao Zhu,[a] Chunsen Liu[b] and Huan Pang*[a]

The rational design of heteroatom-doped C_3N_4 offers a great opportunity to optimize C_3N_4 performance. In this communication, we propose a facile method to fabricate layered-stacked B-doped C_3N_4 (BCN-800) ultrathin nanosheets via one-step calcination route. The distinctive layered-stacked structure and the presence of B atoms provide an active attachment point for antibodies and antigens. In addition, the presence of C and N might aid stability and increase conductivity. When used for vomitoxin detection, the BCN-800-based electrochemical biosensor exhibits high sensitivity with a detection limit of 0.32 pg mL^{-1} and superior selectivity to other interfering agents.

Introduction

Two-dimensional g-C_3N_4 nanosheets have attracted tremendous attention owing to their specific surface area,[1-4] high electron transport ability, significant reduced triplet-triplet annihilation process,[5–7] and potential applications.[8-11] To enhance its electrochemical activity, non-metal heteroatoms,[12,13] i.e., boron (B),[14,15] phosphor and sulfur,[16-19] were doped into g-C_3N_4. In particular, B and C belong to the same cycle and are located in an adjacent location on the periodic table, so they have many similar properties. In addition, functional groups with a B-C bond can act as Lewis acid sites. Based on this advantage, B-doped-C_3N_4 (BCN) have been reported by various research groups.[20] The Liu group reported a B-doped graphitic heptazine-C_3N_4 and applied to visible water splitting.[21] Gao et al. and Yan et al. synthesized BCN nanonanosheets using H_3BO_3 as precursors in a closed environment.[26,27] However, these studies needed to utilize other substances (such as H_3BO_3, B_2O_3) as a boron source and then calcination the as-prepared precursor to obtain the B-doped-C_3N_4 materials. Therefore, a convenient and simple synthesis method needs further development.

Vomitoxin is a highly toxic secondary metabolite found in poorly stored provisions and the allowable amount in human food is 1 ppm.[24,25] The reason vomitoxin is poisonous is that vomitoxin binds to ribosomes, thereby inhibiting protein and nucleic acid formation, and restrains cellular kinases, reducing cell proliferation.[26] Excessive intake of vomitoxin may cause damage to the human body. Therefore, in order to ensure food safety, an efficient and feasible method is needed to detect vomitoxin. Du and co-workers synthesized Al-MOF materials to detect vomitoxin in wine.[27] As far as we know, the application of BCN to food quality testing has not been reported.

For that reason, there is an urgent need to find a novel electrochemical immunosensors to ensure that toxic and harmful materials in the food supply are limited. In this work, we synthesized BCN nanosheets using 4-pyridylboronic acid as both a boron source and a nitrogen source, and not introduce extra impurities through the self-doped process. This work aims to provide an innovative material to specifically detect traces of targeted analytes. There are currently three benefits to this approach: (i) BCN nanosheets are non-metallic materials with low toxicity and high stability; (ii) BCN nanosheets are successfully synthesized via one-step calcination treatment; and (iii) BCN-800 exhibits high sensitivity, selectivity, and stability both antibody and antigen recognition.

Results and discussion

The one-step calcination method for producing BCN-700, BCN-800, and BCN-900 (700, 800, and 900 °C, respectively) is shown in Scheme 1. A detailed description can be found in the Experimental Section (Supporting Information). The morphology and structural features of the BCN-800 were analyzed via scanning electron microscopy (SEM) and TEM

[a] School of Chemistry and Chemical Engineering, Guangling College, Yangzhou University, Yangzhou, 225009, Jiangsu, P. R. China
[b] Henan Provincial Key Lab of Surface & Interface Science, Zhengzhou University of Light Industry, Zhengzhou, Henan 450002, China
E-mail: huanpangchem@hotmail.com; panghuan@yzu.edu.cn
†Electronic supplementary information (ESI) available. See DOI: 10.1039/x0xx00000x

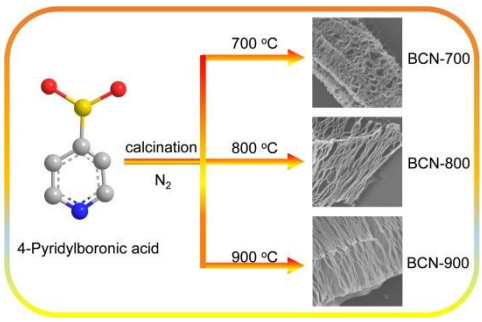

Scheme 1 A simple synthesis scheme of the ultrathin two-dimensional BCN nanosheet.

(transmission electron microscopy). BCN-800 tended to exhibit a layered-stacked ultrathin nanosheet structure as observed in Figure 1a. This layered-stacked ultrathin nanosheet structure may be a result of the melting, dehydration, and precursor evaporation processes of 4-pyridylboronic acid occurring at high temperatures. For comparison, we also prepared BCN-700 and BCN-900. The corresponding SEM and TEM images of BCN-700 and BCN-900 are shown in Figure S1 and Figure S2, respectively. Both have a similar layered-stacked ultrathin nanosheet structure. From the high-resolution TEM (HRTEM) images (Figure 1b and c), the BCN-800 nanosheet not exist obvious lattice fringes, and the SAED pattern is shown in the upper-right inset of Figure 1c. The relevant energy dispersive X-ray spectroscopy (EDX) was further utilized to detect the presence of B, C, N, O elements (Figure 1d).

The X-ray diffraction (XRD) patterns of the three as-prepared BCN are similar to the formerly prepared BCN (Figure S4).[28] The two characteristic peaks are clearly observable: 14.62 °, 27.96 ° (BCN-700); 14.56 °, 27.94 ° (BCN-800); 14.58 °, 27.94 ° (BCN-900). The results also show that those three samples are the same substances. As shown in the Raman spectrum (Figure S5), I_D/I_G increases as the calcination temperature increases, which indicates higher defect density and disorder degree of BCN materials. This is caused by the functional groups formed during the pyrolysis of 4-pyridylboronic acid, such as C-NB, B-N which can be covalently attached to the antibody and provide favorable environments for antibody immobilization.[29]

To investigate the chemical states of B in the samples obtained under different calcination conditions, XPS analysis, was carried out. Figure S6a displays the peak position of oxygen,

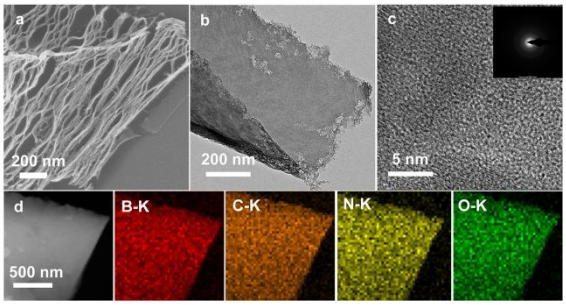

Figure 1 (a) SEM image of BCN-800. (b, c) HRTEM images of BCN-800. (d) EDX elemental mapping images of B, C, N, and O in the BCN-800.

nitrogen, carbon, and boron in BCN materials, respectively, which suggested that BCN nanosheets were successfully formed. Three different peaks are observed in the high-resolution B 1s spectra (Figure S6b), and the peaks centered at *ca.* 192.7, 192.8, and 193.0 eV correspond to BCN-700, BCN-800, and BCN-900, respectively, which is in line with previous reported C-NB group (192.1 eV) of BCN materials.[30] The peaks at 190.0 eV, 190.4 eV, 190.2 eV correspond to the B-C bond.[28] Other peaks at 194.2, 194.4,195.1 eV are attributed to the boron bond of the 4-pyridylboronic acid.

The adsorption of the antibody and antigen for the detection process are shown in Scheme S1. In the performance testing, we assessed the immunosensor performance of the BCN-800 modified AE electrode in electrolyte solution at various stages. As shown in Figure 2a, the CV curves of the bare AE show a pair of obvious redox peaks with peak-to-peak separation (ΔE_p) of 165 mV, showing the electron transfer of the $[Fe(CN)_6]^{3-/4-}$ couple. When the electrode was decorated with BCN-800, the ΔE_p increased to 224 mV, and the redox peak decreased, indicating the reduction of conductivity after BCN-800 modification compared to bare AE, indicating that the electron transfer of $[Fe(CN)_6]^{3-/4-}$ at the electrode surface was hindered by the coverage of BCN-800. The BCN-800/AE electrode was then soaked in antibody$_{vomitoxin}$ (Anti$_{vomitoxin}$) solution for 2 h, the $[Fe(CN)_6]^{3-/4-}$ redox peaks decreasing, and the ΔE_p value increasing (ΔE_p = 311 mV) suggested that the influence of Anti$_{vomitoxin}$ does significantly impact the BCN-800 reduction potential. However, when the prepared Anti$_{vomitoxin}$/BCN-800/AE electrode was used to detect 0.001 ng mL^{-1} vomitoxin solution, the redox peak decreased (ΔE_p = 413 mV), suggesting vomitoxin successfully integrated with the Anti$_{vomitoxin}$/BCN-800/AE. The results suggested that vomitoxin was successfully captured by Anti$_{vomitoxin}$/BCN-800/AE through the immunoreaction between antibody and antigen. Two other BCN materials (BCN-700, BCN-900) displayed similar CV curves (Figure S8 and S9). The ΔE_p of BCN-700 for each of the four stage AE forms described above are 151, 208, 250, and 350 mV, respectively. The ΔE_p of BCN-900 for each of the four stage AE forms described above are 126, 222, 227, 293 mV, respectively. As a result, the antibody adsorption and the vomitoxin detection increasing the non-conductive sensing layer thickening and hindered the electron transfer ($[Fe(CN)_6]^{3-/4-}$) between the electrode surface and the electrolyte solution.[31,32] The result showed that each of the three BCN-based immunosensors were able to successively detection vomitoxin.

Based on Electrochemical Impedance Spectroscopy (EIS) plots (Figure 2b), the R_{ct} values of bare AE is 140 Ω. When bare AE was modified with BCN-800, the impedance curves of BCN-800/AE contains a larger semiarc, and the R_{ct} value increased to 575 Ω. This result revealed the presence of BCN-800 results in comparatively poor conductivity. After soaking BCN-800/AE in Anti$_{vomitoxin}$ solution, to produce Anti$_{vomitoxin}$/BCN-800/AE, the R_{ct} value increased to 1290 Ω. This result is attributed to the electrode surface forming a layer of protein film and impeding

electron transfer in the process. Due to the specific structure, the antibody could penetrate into the interior of the BCN-800 nanocomposites, and the large amounts of antibody could block the surface of the BCN-800/AEs and further decrease the charge transfer.[33] Therefore, the obstructing and blocking effects of antibody result in the substantial decrease of the electrochemical response of BCN-800. After soaking $Anti_{vomitoxin}$/BCN-800/AE in vomitoxin solution, the R_{ct} values of vomitoxin/$Anti_{vomitoxin}$/BCN-800/AE was 1670 Ω. The EIS plots of BCN-700 and BCN-900 are also shown in Figure S10 and Figure S11. The R_{ct} values of BCN-700 for the four stages of AE are 175, 785, 1181, and 1540 Ω, respectively. The R_{ct} values of BCN-900 for the four stages of AE are 39, 160, 305, and 425 Ω, respectively. The EIS results demonstrate that the electron transfer kinetics process is consistent with the corresponding CV curve. The entire process demonstrates that BCN-700, BCN-800, and BCN-900 can act as electrochemical immunosensors with outstanding target molecule recognition capabilities. Figure S12 shows the change in value of R_{ct} (ΔR_{ct}) of each step of BCN-700, BCN-800, and BCN-900 toward vomitoxin detection. The quantity of $Anti_{vomitoxin}$ adsorbed to the surface of BCN-800/AE is greater than the other two materials, which is attributed to the appropriate defect density and disorder degree of BCN-800. Besides, from Table S3, the boron content decreases with the temperature increases, and follows the order: BCN-900<BCN-800<BCN-700. Due to the different atomic radius and electronic density, the substitution of C/N by B would generate some defects in the BCN structure. Defects that are too high or too low are not conducive to the adsorption of the antibody. Thus, the BCN-800 exhibits the superior performance, suggesting that there exists an optimal doping content of B.[34] A large amount of antibody means high detection efficiency for the antigen,[35] further resulting in the maximum ΔR_{ct} ($R_{ct,\ Antivomitoxin} - R_{ct,\ material}$) and ΔR_{ct} ($R_{ct,\ 0.001\ ng\ mL^{-1}\ vomitoxin} - R_{ct,\ Antivomitoxin}$) for BCN-800.

For further performance analysis, more EIS data were acquired by immersing the $Anti_{vomitoxin}$/BCN-800/AE electrode in the different concentrations of vomitoxin solution. Figure 3a illustrates the Nyquist plots of $Anti_{vomitoxin}$/BCN-800/AE for detection of different vomitoxin concentrations. The R_{ct} values increases as the concentrations of vomitoxin increases (0.001, 0.005, 0.01, 0.05, 0.1, 0.5 ng mL^{-1}), which corresponds to more antigen-antibody binding on the BCN-based immunosensors

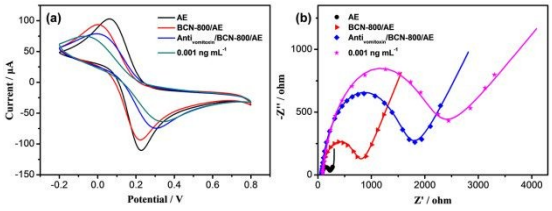

Figure 2 (a) CV at a scan rate of 100 mV s^{-1} (b) EIS plots tracing the whole procedure of vomitoxin detection using the developed biosensor based on BCN-800, in 5 mM $[Fe(CN)_6]^{3-/4-}$ containing 0.14 M NaCl and 0.1 M KCl: AE, BCN-800/AE, $Anti_{vomitoxin}$/BCN-800/AE, 0.001 ng mL^{-1} vomitoxin.

surface, and the resistance increases during $[Fe(CN)_6]^{3-/4-}$ electron transfer. The ΔR_{ct} before and after the immunoreaction is proportional to the logarithm of the vomitoxin concentration(0.001-0.5 ng mL^{-1}), and the ΔR_{ct} can be used as a sensing signal of immunoreaction. The linear regression equation was $\Delta R_{ct} = 2.316 + 0.661 LogC_{vomitoxin}$, with the correlation coefficient (R^2) of 0.990 (Figure 3b). The detection limit (LOD) was estimated to be 0.32 pg mL^{-1} (signal-to-noise ratio = 3). To verify the universality of the BCN-800-based detection system, we further detection of harmful substances (salbutamol) in food. As shown in Figure S15, the peak current continuous decrease in the testing process (Figure S15a) and R_{ct} values increasing with the BCN-800 bio-binding to the $Anti_{salbutamol}$ and salbutamol (Figure S15b), indicating the antibody adsorption and the salbutamol detection hindered the electron transfer between the electrode surface and the electrolyte solution. Thus, the developed electrochemical immunosensors based on BCN-800 can be used to monitor the fields of environmental protection and serve as a potential strategy to determine food safety. As showing in Figure S16, the linear regression equation was $\Delta R_{ct} = 2.466 + 0.693 LogC_{salbutamol}$, with the correlation coefficient (R^2) of 0.991. The LOD was estimated to be 0.28 pg mL^{-1}. Additionally, the analytical performances of the developed biosensors based on BCN-800 in detecting vomitoxin and salbutamol were superior to those of other reported biosensors (Table S2).

Doxycycline (DOX), streptomycin, oxytetra, ofloxacin, and penicillin (1.0 ng mL^{-1}) were used as interfering agents to examine the immunosensor's selectivity. Figure S13 shows the R_{ct} responses for the five antigens, and no significant changes were obtained with the addition these interfering agents compared to the significant response of the ΔR_{ct} values observed for the vomitoxin detection. The results show the high selectivity of immunosensors for vomitoxin over other antigens due to the high specific recognition between vomitoxin and its corresponding antibody. The reproducibility of the five BCN-800-based immunosensors was assessed by measuring the ΔR_{ct} values after exposure to the 1.0 pg mL^{-1} vomitoxin solution at 25 °C (Figure S13a). From these measurements, we determined the relative standard deviation (RSD) of the five immunosensors for vomitoxin detection is 4.36%. Moreover, the BCN-800-based immunosensor was maintained at 4 °C for 12 days testing R_{ct} values, and the R_{ct} response presented only a minor shift (2.13%) compared to the first measurement for vomitoxin detection (Figure S14), which indicates superior stability and storage performance. Obviously, BCN-800 exhibits excellent precision,

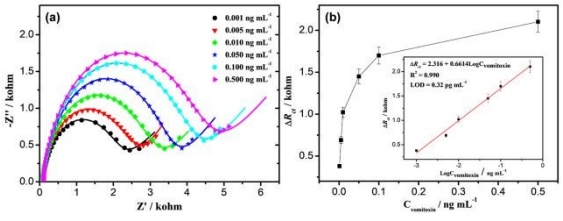

Figure 3 (a) EIS responses of the $Anti_{vomitoxin}$/BCN-800/AE with different concentrations of vomitoxinn (0.001, 0.005, 0.01, 0.05, 0.1, and 0.5 ng mL^{-1}); (b) Dependence of ΔR_{ct} of the

modified electrode on concentration of vomitoxin. The linear part of the calibration curve is shown in the inset of (b). reproducibility, and stability as a sensor.

Through testing the applicability of BCN-800-based immunosensor toward vomitoxin in a wine sample, showing an acceptable recoveries of 97.0-100.3% for vomitoxin detection (Table S1). The result indicates that the BCN-800-based immunosensor can be applied to vomitoxin detection in real samples.

Conclusions

In summary, we suggested a facile strategy to fabricate a series of BCN composites by controlling the calcination temperature (700, 800, 900 ^{o}C), which serve as an immunosensing system for detecting vomitoxin. This strategy uses 4-pyridylboronic acid as the only boron and nitrogen source. Through this simple synthetic strategy, BCN-800 reserves the advantages of the non-mentallic, B-doped, and unique layered structure and enhances antibody adsorption and antigen detection. Compared with the other two samples, the defect density and disorder degree of BCN-800 is between BCN-700 and BCN-900, which will not cause higher defect density nor more disorder degree. In addition, the ratio of C, N, B content of BCN-800 is also between BCN-700 and BCN-800. It is because of the existence of this intermediate state that BCN-800 material has better electrochemical performance. Moreover, the layered-stacked BCN-800 ultrathin nanosheets show excellent selectivity and sensitivity for detecting as little as 1.0 pg mL^{-1} vomitoxin. This approach may provide a new strategy for improving the synthesis of B-doped-C_3N_4.

Conflicts of interest

There are no conflicts to declare

Acknowledgements

This work was supported by the Program for New Century Excellent Talents of the University in China (NCET-13-0645) and the National Natural Science Foundation of China (NSFC-21201010, 21671170 and 21673203), the Six Talent Plan (2015-XCL-030), and Qinglan Project. We also acknowledge the Priority Academic Program Development of Jiangsu Higher Education Institutions and the technical support we received at the Testing Center of Yangzhou University.

References

1 W. Yang, X. Li, Y. Li, R. Zhu, H. Pang, *Adv. Mater.* 2018, **31**, 1804740.

2 X. Zhao, H. Chen, F. Kong, Y. Zhang, S. Wang, S. Liu, L. A. Lucia, P. Fatehi, H. Pang, *Chem. Eng. J.* 2019, **364**, 226.

3 Y. Zhao, L. Yang, S. Chen, X. Wang, Y. Ma, Q. Wu, Y. Jiang, W. Qian, Z. Hu, *J. Am. Chem. Soc.* 2013, **135**, 1201.

4 C. Zhou, Y. Ren, J. Han, X. Gong, Z. Wei, J. Xie, R. Guo, *J. Am. Chem. Soc.* 2018, **140**, 9417.

5 H. Wang, S. Jiang, S. Chen, X. Zhang, W. Shao, X. Sun, Z. Zhao, Q. Zhang, Y. Luo, Y. Xie, *Chem. Sci.* 2017, **8**, 4087.

6 P. Niu, L. Zhang, G. Liu, H. Cheng, *Adv. Funct. Mater.* 2012, **22**, 4763.

7 F. Wang, Y. Liu, Y.F. Zhao, Y. Wang, Z.J. Wang, W.H. Zhang, F.Z. Ren, *Appl. Sci.-Basel* 2018, **8**.

8 S. Yang, Y. Gong, J. Zhang, L. Zhan, L. Ma, Z. Fang, R. Vajtai, X. Wang, P. M. Ajayan, *Adv. Mater.* 2013, **25**, 2452.

9 J. Liu, Y. Liu, N. Liu, Y. Han, X. Zhang, H. Huang, Y. Lifshitz, S. Lee, J. Zhong, Z. Kang, *Science* 2015, **347**, 970.

10 C. Pan, J. Xu, Y. Wang, D. Li, Y. Zhu, *Adv. Funct. Mater.* 2012, **22**, 1518.

11 X. Zhang, X. Xie, H. Wang, J. Zhang, B. Pan, Y. Xie, *J. Am. Chem. Soc.* 2013, **135**, 18.

12 S. Gong, W. Wan, S. Guan, B. Tai, C. Liu, B. Fu, S. A. Yang, Y. Yao, *J. Mater. Chem. C* 2017, **5**, 8424.

13 Y. Cui, G. Zhang, Z. Lin, X. Wang, *Appl. Catal. B Environ.* 2016, **181**, 413.

14 N. Sagara, S. Kamimura, T. Tsubota, T. Ohno, *Appl. Catal. B Environ.* 2016, **192**, 193.

15 Z. Lin, X. Wang, *Angew. Chemie Int. Ed.* 2013, **52**, 1735.

16 Y. Zhou, L. Zhang, J. Liu, X. Fan, B. Wang, M. Wang, W. Ren, J. Wang, M. Li, J. Shi, *J. Mater. Chem. A* 2015, **3**, 3862.

17 X. Wang, C. Yang, X. Xiong, G. Chen, M. Huang, J.-H. Wang, Y. Liu, M. Liu, K. Huang, *Energy Storage Mater.* 2019, **16**, 344.

18 J. L. Ma, J. B. Wen, Q. A. Li, Q. Zhang, *INT J HYDROGEN ENERG* 2013, **38**, 14896.

19 M. Seredych, T. J. Bandosz, *Carbon* 2016, **107**, 895.

20 T. Bhowmik, M. K. Kundu, S. Barman, *ACS Catal.* 2016, **6**, 1929.

21 H. Yu, X. Jiang, Z. Shao, J. Feng, X. Yang, Y. Liu, *Nanoscale Res. Lett.* 2018, **13**, 57.

22 D. Gao, Y. Liu, P. Liu, M. Si, D. Xue, *Sci. Rep.* 2016, **6**, 35768.

23 Q. Yan, G.-F. Huang, D. Li, M. Zhang, A. Pan, W. Huang, *J. Mater. Sci. Technol.* 2018, **34**, 2515.

24 L. Pinotti, M. Ottoboni, C. Giromini, V. Dell'Orto, F. Cheli, *Toxins (Basel).* 2016, **8**, 45.

25 D. Shi, R. Zheng, M.-J. Sun, X. Cao, C.-X. Sun, C.-J. Cui, C.-S. Liu, J. Zhao, M. Du, *Angew. Chemie Int. Ed.* 2017, **56**, 14637.

26 W. Gu, P. Zhu, D. Jiang, X. He, Y. Li, J. Ji, L. Zhang, Y. Sun, X. Sun, *Biosens. Bioelectron.* 2015, **70**, 447.

27 C. Liu, C. Sun, J. Tian, Z. Wang, H. Ji, Y. Song, S. Zhang, Z.-H. Zhang, L.-H. He, M. Du, *Biosens. Bioelectron.* 2017, **91**, 804.

28 Z. Wang, M. Chen, Y. Huang, X. Shi, Y. Zhang, T. Huang, J. Cao, W. Ho, S. C. Lee, *Appl. Catal. B Environ.* 2018, **239**, 352.

29 S. Balamurugan, A. Obubuafo, S. A. Soper and D. A. Spivak, *Anal. Bioanal. Chem.*, 2008, **390**, 1009.

30 M. Kawaguchi, 1996, **4756**, 1197.

31 L. J. Yang, Y. B. Li, *Biosens. Bioelectron.* 2005, **20**, 1407.

32 C. Ruan, L. Yang, Y. Li, *Anal. Chem.* 2002, **74**, 4814.

33 F. Yuan, H. Zhao, X. Wang and X. Quan, *Anal. Lett.* 2017, **50**,544.

34 L. Gomathi, R. Kavitha, *Appl Catal B: Environ* 2013, **140-141**, 559.

35 P. He, L. Shen, Y. Cao, D. Li, *Anal. Chem.* 2007, **79**, 8024.

View Article Online
DOI: 10.1039/C9CC03787J

Table of Contents

Boron-doped carbon nitride are synthesized as biosensing platforms for assessment of food safety, which derived from 4-pyridylboronic acid precursor. The BCN-800-based electrochemical biosensor exhibits high sensitivity with a detection limit of 0.32 pg mL^{-1} and superior selectivity toward other interfering agents.